Light-induced formation of NO in endothelial cells by photoactivatable NADPH analogues targeting nitric-oxide synthase

Rahima Chennoufi, Aimeric Cabrié, Nhi Ha Nguyen, Nicolas Bogliotti, Françoise Simon, Bertrand Cinquin, Patrick Tauc, Jean-Luc Boucher, Anny Slama-Schwok, Juan Xie, et al.

Light-induced formation of NO in endothelial cells by photoactivatable NADPH analogues targeting nitric-oxide synthase

Rahima Chennoufi[a], Aimeric Cabrié[a], Nhi Ha Nguyen[b], Nicolas Bogliotti[b], Françoise Simon[a], Bertrand Cinquin[a], Patrick Tauc[a], Jean-Luc Boucher[c], Anny Slama-Schwok[d], Juan Xie[b], Eric Deprez[a,*]

[a]*LBPA, CNRS UMR8113, IDA FR3242, ENS Paris-Saclay, Université Paris-Saclay, F-94235 Cachan, France*
[b]*PPSM, CNRS UMR8531, IDA FR3242, ENS Paris-Saclay, Université Paris-Saclay, F-94235 Cachan, France*
[c]*Laboratoire de "Chimie et Biochimie Pharmacologiques et Toxicologiques", CNRS UMR8601, Université Paris Descartes, 75270 Paris, France*
[d]*Laboratoire de "Stabilité Génétique et Oncogénèse", CNRS UMR8200, Gustave Roussy, Université Paris-Saclay, 94607 Villejuif, France*

[*]Corresponding author: deprez@lbpa.ens-cachan.fr

Abbreviations: BH_4, tetrahydrobiopterin; DIC, Differential Interference Contrast; FAD, Flavin Adenine Dinucleotide; FMN, Flavin Mononucleotide; GM, Göppert-Mayer; H_2DCF-DA, 2',7'-dichlorodihydrofluorescein; HUVECs, Human Umbilical Vein Endothelial Cells; L-NAME, N^{ω}-nitro-L-arginine methyl ester; MTT, 3-(4,5-dimethylthiazol-2-yl)-2,5-diphenyltetrazolium bromide; NAC, N-acetyl cysteine; NADPH, Nicotinamide Adenine Dinucleotide Phosphate; NO, Nitric-oxide; e/n/iNOS, Nitric-oxide synthase (e: endothelial; n: neuronal; i: inducible); PMT, Photomultiplier tube; ROS, Reactive Oxygen Species; t-BHP, Tert-butyl hydroperoxide; Φ_F, fluorescence quantum yield; σ^2, two-photon absorption cross-section.

ABSTRACT

Background: Nitric-oxide synthases (NOS) catalyze the formation of NO using NADPH as electron donor. We have recently designed and synthesized a new series of two-photon absorbing and photoactivatable NADPH analogues (NT). These compounds bear one or two carboxymethyl group(s) on the 2'- or/and 3'-position(s) of the ribose in the adenosine moiety, instead of a 2'-phosphate group, and differ by the nature of the electron donor in their photoactivatable chromophore (replacing the nicotinamide moiety). Here, we addressed the ability of NTs to photoinduce eNOS-dependent NO production in endothelial cells.
Methods: The cellular fate of NTs and their photoinduced effects were studied using multiphoton fluorescence imaging, cell viability assays and a BODIPY-derived NO probe for NO measurements. The eNOS dependence of photoinduced NO production was addressed using two NOS inhibitors (NS1 and L-NAME) targeting the reductase and the oxygenase domains, respectively.
Results: We found that, two compounds, those bearing a single carboxymethyl group on the 3'-position of the ribose, colocalize with the Golgi apparatus (the main intracellular location of eNOS) and display high intracellular two-photon brightness. Furthermore, a eNOS-dependent photooxidation was observed for these two compounds only, which is accompanied by a substantial intracellular NO production accounting for specific photocytotoxic effects.
Conclusions: We show for the first time that NT photoactivation efficiently triggers electron flow at the eNOS level and increases the basal production of NO by endothelial cells.
General significance: Efficient photoactivatable NADPH analogues targeting NOS could have important implications for generating apoptosis in tumor cells or modulating NO-dependent physiological processes.

Keywords: two-photon absorption probes; nitric-oxide synthase activator; photoactivation; photo-induced electron transfer; endothelial cells; cell death.

1. Introduction

Nitric-oxide (NO) is a key cellular signaling mediator involved in the overall regulation of physiological homeostasis and in numerous pathological processes related to cardiovascular, nervous and immune systems [1-4]. NO is formed together with L-citruline by nitric-oxide synthases (NOS) that catalyze the oxidation of L-arginine using nicotinamide adenine dinucleotide phosphate (NADPH), flavin adenine dinucleotide (FAD), flavin mononucleotide (FMN), tetrahydrobiopterin (BH_4) and O_2 as cofactors [5,6]. The overall catalytic process is driven by reducing equivalents supplied by NADPH. NOS are composed of a reductase domain which binds NADPH and the two flavins and an oxygenase domain which binds the heme, L-arginine, BH_4 and O_2; these two domains are connected by the calmodulin-binding domain. The electron flow leading to the formation of NO is initiated by the binding of NADPH to the reductase domain and requires the binding of calmodulin for efficient FMN→heme electron transfer [5-8].

NO is produced by three NOS isoforms, the two first are constitutive, neuronal (nNOS) and endothelial (eNOS) whereas the third one is inducible (iNOS). Dysregulation of NO production (negative or positive) can lead to several disorders and could be counteracted by strategies aiming at modulating the NO level, by activating or inhibiting NOS. This is well illustrated for instance considering NO produced by eNOS in the vascular endothelium which plays important roles in regulating vascular tone [9]. Although eNOS has a global protective function in the cardiovascular system, it has been also described to participate in tumor initiation and maintenance, and thus has a detrimental effect in this specific context [10,11]. Furthermore, in the cancer context, there is interest to develop both strategies, *i.e.* inhibition and activation of NO formation, to inhibit tumor growth or to induce tumor cell death, respectively [12].

Many efforts have focused on the development of NOS inhibitors. Most of them target the oxygenase domain, mainly L-arginine analoguess, whereas diphenyliodonium and analogues target flavins in the reductase domain [13-16]. Recently, we have designed and characterized a competitive inhibitor of NOS, named NS1 [17]. NS1 is a NADPH analogue that targets the NADPH binding site in the reductase domain and efficiently inhibits NO production *in vitro*, *in cellulo* and in aortic rings [18]. This compound contains the nucleotide recognition part of NADPH linked to a chromophoric moiety that replaces the nicotinamide part of NADPH. The chromophoric moiety displays a typical push-pull structure allowing two-photon fluorescence imaging of NOS in the cell context and a terminal electron acceptor nitro group that (i) blocks the electron flow and NOS catalysis and (ii) modulates the fluorescence quantum yield of NS1 as a function of the environment (weakly fluorescent when free in solution *vs* highly fluorescent when bound to the protein) [17].

On the activation side, most compounds that stimulate NO production do not directly target NOS and correspond to molecular precursors or activators of NOS expression [12,19]. Nevertheless, a prototype compound (NT_1; Fig. 1) that targets the NADPH-binding site of NOS was shown to photoactivate NO production *in vitro* [20,21]. The design of this compound is similar to that described for NS1 except that the terminal nitro group in the chromophoric moiety is replaced by a terminal electron donor amine group ($-NH_2$) in NT_1. This constitutes a photoactivatable chromophore by a one- or two-photon excitation process, compatible with both electron injection to FAD by the excited compound and subsequent NO production.

Recently, we designed a second generation of NT compounds, characterized by good cellular uptake properties ($NT_{2\text{-}x}$: $NT_{2\text{-}2}$—$NT_{2\text{-}9}$; Fig. 1) [22]. The synthesis of these compounds was significantly easier compared to NT_1 thanks to the click chemistry and the substitution on the adenosine moiety of the phosphate group linked to the 2'-carbon of the ribose by one or two carboxymethyl group(s): $NT_{2\text{-}2}$/$NT_{2\text{-}3}$ have two carboxymethyl groups, $NT_{2\text{-}4}$/$NT_{2\text{-}5}$ and $NT_{2\text{-}6}$/$NT_{2\text{-}7}$ have one carboxymethyl group on the 3'- and 2'-carbon, respectively, whereas $NT_{2\text{-}9}$ has no carboxymethyl group. $NT_{2\text{-}2}$—$NT_{2\text{-}9}$ compounds display a terminal electron donor group which is $-NH_2$ (odd numbers) or $-NHCH_3$ (even numbers); they are characterized by (i) good two-photon absorption cross sections with σ^2 values ranging from 30-to-70 GM at 760 nm and (ii) significant fluorescence enhancement upon binding to recombinant NOS as measured *in vitro* [22]. Except $NT_{2\text{-}9}$ which poorly binds to eNOS ($K_d \geq 80$ μM), all 2nd-generation NTs display reasonable affinities for recombinant eNOS, with K_d values in the 15-30 μM range, indicating that the presence of at least one

carboxymethyl group on the ribose is required for a stable NT/NOS interaction and that the nature of the terminal electron donor group is not determinant for efficient binding. In the present study, we addressed the question of the structural determinants for NT-NOS interaction in the cell context by studying the cellular fate of NTs in endothelial cells and we investigated their abilities to photoinduce electron flow at the eNOS level with concomitant intracellular NO production. We report for the first time that photoactivation of NT compounds, more particularly NT_{2-4} and $NT_{2-5,}$ is compatible with electron injection to FAD in the NOS reductase domain and leads to substantial intracellular NO production.

2. Materials and Methods

2.1. Synthesis and reagents

Synthesis of NT_{2-2}—NT_{2-9} was previously described [22]. NTs were stored as powders at -20°C and dissolved to 10 mM before use in dimethyl sulfoxide (DMSO). Stock solutions were kept at -20°C (max. one week). Synthesis of NS1 was previously described [17]. The BODIPY-derived NO probe was synthesized according to Lv *et al.* [23]. N-acetyl cysteine (NAC), N^{ω}-nitro-L-arginine methyl ester (L-NAME), 2',7'-dichlorodihydrofluorescein (H_2DCF-DA), Tert-butyl hydroperoxide (t-BHP), 3-(4,5-dimethylthiazol-2-yl)-2,5-diphenyltetrazolium bromide (MTT) and DMSO were from Sigma-Aldrich.

2.2. Cell cultures

Human Umbilical Vein Endothelial cells (HUVEC; Sigma) were cultured in Petri dishes coated with 0.2% gelatin in Endothelial Cell Growth Medium (ECGM; Cell Application) [17,24]. HeLa cells were cultured in Dulbecco's Modified Eagle's Medium (DMEM; Gibco®) supplemented with 10% Fetal Bovin Serum (Gibco®) and 1% penicillin-streptomycin (Gibco®). HUVEC and HeLa cells were cultured at 37°C (5% CO_2) to ≈95% confluence. HUVECs were used within passage five.

2.3. Two-photon fluorescence imaging of NTs in HUVECs

HUVECs were plated in glass bottom dishes (WillCo-dish; WillCo Wells) and incubated with 5 µM NT for 2h at 37°C (the maximum of NT uptake was reached after 5 min-incubation as previously shown). Two-photon fluorescence images of living HUVECs were obtained using a SP2 confocal microscope (Leica MicroSystems) equipped with an oil immersion x63 objective (NA, 1.32) and an incubation chamber (37°C, CO_2 5%). The excitation source was a 80-MHz mode-locked Mai-Tai Ti:Sapphire tunable laser (720—920 nm, 100-fs laser pulse; Spectra Physics) tuned to 760 nm (emission slit: 450—550 nm). The intracellular fluorescence intensity of NTs was quantified using the ImageJ software.

2.4. Colocalization experiments with the Golgi apparatus

HUVECs were pre-incubated with 5 µM NT for 2h at 37°C. The cells were then washed with PBS buffer (Phosphate-Buffered Saline; Gibco®) and further incubated with 5 µM Golgi tracker (BODIPY TR-ceramide; Molecular Probes) for 1h. NTs were excited as described above (λ_{ex}: 760 nm; emission slit: 450—550 nm) whereas a continuous laser line (543 nm) was used for excitation of the Golgi traker (emission slit: 570—720 nm). The PMT (photomultiplier tube) gain used for the NT channel was 1,000V for NT_{2-2}/NT_{2-3}, 830V for NT_{2-4}, 900V for NT_{2-5}, 980V for NT_{2-7} and 930V for NT_{2-9}. The quantitative evaluation of colocalization was performed by using the Manders' Colocalization Coefficients (MCC): tM1 (= the fraction of the fluorescence signal in the "NT" channel colocalized with a fluorescence signal in the "Golgi traker" channel) and tM2 (=the fraction of the fluorescence signal in the "Golgi traker" channel colocalized with a fluorescence signal in the "NT" channel) [25]. tM1 and tM2 were calculated using the Coloc 2 plugin in Fiji/ImageJ [26].

2.5. Photobleaching of NTs in the cell context and photoinduced membrane blebbing upon two-photon excitation

Living HUVEC or HeLa cells were pre-incubated with 5 μM NT for 2h at 37°C and washed with PBS buffer (phosphate-buffered saline, pH 7.5; Gibco®) before imaging. For experiments in the presence of NAC, NT-treated HUVECs were further incubated with 3 mM NAC for 24h. For experiments in the presence of L-NAME or NS1, NT-treated HUVECs were further incubated with either 100 μM L-NAME for 3h or 20 μM NS1 for 30 min, respectively. NTs were continuously excited in the two-photon excitation mode at 760 nm (irradiance, 1.25 $W.cm^{-2}$) during 15 min. The NT fluorescence emission intensity was recorded in real-time using the Leica confocal software. Images in the Differential Interference Contrast (DIC) transmission mode, allowing direct observation of membrane blebbing, were recorded before and after the 15-min irradiation period. The irradiance was calculated by measuring the power at the exit of the objective using a Vega power meter (Ophir). The power measurement was performed under similar conditions than image acquisition, *i.e.* in the x-y scan mode (image size, 512x512 pixels; field of view, 238x238 μm; scanning frequency, 400 Hz). Fluorescence imaging experiments for reactive oxygen species (ROS) detection were performed with H_2DCF-DA [27,28]. After pre-incubation with NT and two-photon irradiation as mentioned above, HUVECs were treated with 10 μM H_2DCF-DA for 1h. A continuous laser line (488 nm) was used for imaging of DCF (emission slit: 500—530 nm). The positive control experiment for ROS detection was performed using HUVECs pre-incubated with the oxidative stress inducer t-BHP (100 μM) for 3h at 37°C before H_2DCF-DA treatment.

2.6. Cell viability test

HUVECs plated at 95% confluence in 24-well plates coated with 0.2% gelatin (10,000 cells/well) were treated with 1‰ DMSO (v/v) (control) or NT (final concentration: 3 or 5 μM) for 2h at 37°C and further subjected or not to light exposure during 30 min. For experiments performed in the presence of NOS inhibitors, a 30-min pre-incubation step was performed at 37°C in the presence of 100 μM L-NAME or 20 μM NS1. The excitation source was a Mercury-Xenon lamp (Hamamatsu, LC6 Lightningcure, 200W) equipped with an excitation filter centered at 370 nm (±20 nm) (irradiance, 6.6 $mW.cm^{-2}$, measured using a Vega power meter on a total illuminated surface of 2.3 cm^2 (equiv. 1 well)). After further incubation of treated cells in the dark for 24h at 37°C, cell viability was determined by a colorimetric MTT assay [27]. The absorbance at 570 nm was measured using a VictorTM X5 microplate reader (Perkin Elmer).

2.7. Measurement of NO production upon NT photoactivation in HUVECs

NO production was measured on cell extracts from NT-treated and photo-irradiated HUVECs using a BODIPY-derived NO probe [23]. HUVECs were plated at 95% confluence in gelatin-coated Petri dishes (diameter, 35 mm). The ECGM was phenol red free. The cells were simultaneously treated with NT (5 μM) and the BODIPY-derived NO probe (0.5 or 5 μM) for 1h at 37°C (for experiments in the presence of NOS inhibitors, a 30-min pre-incubation step was performed at 37°C in the presence of 100 μM L-NAME or 20 μM NS1). The cells were then subjected or not to light exposure during 30 min (the excitation source was a 200W Mercury-Xenon lamp equipped with an excitation filter: 370±20 nm). The irradiance was 1.6 $mW.cm^{-2}$ (measured using a Vega power meter on a total illuminated surface of 9.6 cm^2). After illumination and removal of the ECGM, the cells were first incubated in the cell lysis buffer (50 mM Tris-HCl, pH 7.5, 150 mM NaCl, Triton X-100 1%) for 20 min at room temperature and then, centrifuged to eliminate cell debris (10 min at 12,000g). The fluorescence of the BODIPY-derived NO probe was measured at 37°C in the supernatant (cell lysate) using an Eclipse (Varian) spectrofluorometer equipped with a thermostated cell holder. Fluorescence emission spectra were recorded between 500 and 600 nm (λ_{ex}: 480 nm; $\Delta\lambda_{ex} = \Delta\lambda_{em}$ = 10 nm; PMT = 600 or 750V for samples containing 5 or 0.5 μM of NO probe, respectively). For each condition, the total fluorescence intensity of the NO probe was calculated in the 500-530 nm range. To take into account the fluorescence emission of NS1 in the 500-530 nm range upon excitation at 480 nm (≈3%

and 16% of the total fluorescence intensity using PMT = 600V and 750V, respectively), emission spectra of the NO probe in NS1-treated samples were systematically corrected from the NS1 emission contribution (measured using the same setting on cell extracts of HUVECs treated with NS1 only). In these conditions, optimal excitation and emission wavelengths of NS1 were 451 and 613 nm, respectively.

2.8. Statistical Analysis

Statistical significance in Fig. 4 and Fig. 7 was determined using the paired t-test and two-way ANOVA (GraphPad Prism 5).

3. Results and discussion

There is increasing interest in the use of exogenous compounds/systems or genetically encoded transactivators that photoactivate intracellular enzymatic reactions or gene expression [29-32]. Among the light-induced catalytic processes, many efforts have been made to develop chemical compounds/nanomaterials that photoactivate enzymes by initiating electron transfer [32,33]. Here, we address the possibility that the photoactivation of new NT compounds ($NT_{2\text{-}x}$) directly trigger electron transfer through eNOS and might lead to the intracellular production of NO.

3.1. Two-photon fluorescence imaging of NTs and insight into their subcellular localization in living endothelial cells

Our previous study suggested that NT compounds display inhomogeneous behaviors in terms of fluorescence intensity, depending on both the nature of the compound and the cell type [17]. Here, we quantified intracellular fluorescence intensity (upon two-photon irradiation at 760 nm) for each NT in two distinct cellular context: endothelial (HUVEC) and HeLa cells, expressing or not eNOS, respectively [17,22]. Among the different compounds of the $NT_{2\text{-}x}$ series, only $NT_{2\text{-}4}$/$NT_{2\text{-}5}$ led to a strong intracellular two-photon brightness when incubated with living HUVECs (Fig. 2A-B), but not with cells not expressing eNOS such as HeLa cells (Fig. S1), suggesting that $NT_{2\text{-}4}$ and $NT_{2\text{-}5}$ could specifically target eNOS in HUVECs.

The highest two-photon fluorescence intensity of $NT_{2\text{-}4}$ and $NT_{2\text{-}5}$ observed in HUVECs was not predicted by the affinities of NT-eNOS complexes as determined *in vitro* with recombinant eNOS [22], nor by the two-photon brightness hierarchy as derived from *in vitro* measurements (see $\sigma^2 x \Phi_F$ values in Fig. 1). Indeed, the two-photon brightness of $NT_{2\text{-}x}$ in HUVECs upon excitation at 760 nm follows a hierarchy ($NT_{2\text{-}4}$/$NT_{2\text{-}5}$ > $NT_{2\text{-}9}$ >> $NT_{2\text{-}2}$ > $NT_{2\text{-}3}$/$NT_{2\text{-}7}$) (Fig. 2) that is clearly distinct than the one established from values measured *in vitro* ($NT_{2\text{-}3}$ > $NT_{2\text{-}4}$ > $NT_{2\text{-}2}$ > $NT_{2\text{-}7}$ > $NT_{2\text{-}5}$ > $NT_{2\text{-}9}$) (Fig. 1). Such an apparent discrepancy could be related to distinct subcellular localizations/local environments of NTs that could differentially influence their intrinsic fluorescence property. To get deeper insight into the NT subcellular localization in living HUVECs, colocalization experiments were then carried out using the BODIPY TR-ceramide Golgi tracker since the Golgi apparatus represents the main subcellular location of eNOS together with the plasma membrane [34,35]. As shown in Fig. 2C-D, the strongest colocalization signals were obtained with $NT_{2\text{-}4}$/$NT_{2\text{-}5}$ (MCC = 0.53-0.66), whereas only weak/moderate colocalization signals of $NT_{2\text{-}7}$/$NT_{2\text{-}9}$ were detected (MCC = 0.37-0.45). $NT_{2\text{-}2}$/$NT_{2\text{-}3}$ did not or very weakly colocalize with the Golgi apparatus (MCC = 0.22-0.31). This result suggests a relationship between the NT/Golgi colocalization and the two-photon brightness of NTs in the cell context. Unfortunately, a direct NT/eNOS colocalization was not possible to perform due to a systematic delocalization of $NT_{2\text{-}4}$/$NT_{2\text{-}5}$ (not shown) during cell fixation that is required for specific immunostaining of eNOS [17]. The specific targeting of eNOS by $NT_{2\text{-}4}$/$NT_{2\text{-}5}$ was then further investigated in the cell context by using NOS inhibitors in two-photon photoactivation experiments.

3.2. The two-photon photoactivation of $NT_{2\text{-}4}$/$NT_{2\text{-}5}$ leads to cell death in an eNOS-dependent manner

HUVECs were pre-treated with NTs and then, subjected to continuous two-photon irradiation during 15 min. The images obtained in the DIC transmission mode highlight important morphological changes of cells upon illumination, specifically those treated with NT_{2-4}/NT_{2-5} (Fig. 3). These morphological changes include cell shrinkage and formation of plasma membrane blebs, corresponding to morphological hallmarks of apoptosis following phosphatidylserine externalization at the plasma membrane level [36,37]. By contrast, untreated cells or cells incubated with other NTs did not lead to any significant morphological change or cell death upon illumination. Cell viability (MTT) tests confirmed that the observation of membrane blebbing upon prolonged illumination of NTs in HUVECs accounts for cell death and that cell death occurs specifically upon NT_{2-4}/NT_{2-5} photoactivation (Fig. 4). In the absence of NT, the irradiation treatment alone did not induce significant cell death. NT_{2-7} did not show any toxic effect at 3 μM whereas a significant toxic effect was observed at 5 μM, but not dependent on light irradiation. By contrast, NT_{2-4} and NT_{2-5} led to significant photocytotoxic effects at both concentrations, confirming conclusions based on the observation of cell morphological changes (Fig. 3). For both compounds, the photocytotoxicity was significantly higher than the dark toxicity, regardless of the concentration (3 or 5 μM). To note, NT_{2-5} displayed a higher dark toxicity than NT_{2-4} (100% and 94% of cell viability in the presence of 3 and 5 μM NT_{2-4}, respectively, compared with 92% and 78.5% of cell viability in the presence of 3 and 5 μM NT_{2-5}, respectively). At this stage, the mechanism behind the phototoxicity could be related to the formation of ROS upon NT photoactivation, independently of eNOS. Alternatively, the cell death process could also rely on NT photoactivation at the NOS level. We favor this second hypothesis since there is a strong parallel between the ability of these two NTs to photoinduce cell death and their respective localization at the Golgi level, although the nature of the molecular messenger involved in the cell death process remains uncertain; indeed, the NT_{2-4}/NT_{2-5} photoactivation could trigger electron flow through eNOS, leading to either ROS production, originating from electron leakage [38,39], or NO production that can also initiates cell apoptosis [40,41].

Importantly, the light-dependent formation of membrane blebs in NT_{2-4}/NT_{2-5}-treated HUVECs was not counteracted by the presence of the antioxidant N-acetyl cysteine (NAC) (Fig. 5A) and no ROS formation consecutive to light illumination was observed using the ROS detector H_2DCF-DA (Fig. S3) [27,28,42]. By contrast, membrane blebbing was significantly counteracted by two different NOS inhibitors, L-NAME and NS1 (Fig. 5B-C), that target the oxygenase domain and the NADPH-binding site in the reductase domain, respectively [14,17]. Moreover, a significant protective effect of L-NAME or NS1 against the photocytotoxicity of NT_{2-4}/NT_{2-5} was consistently observed in MTT assays (Fig. 4). Both compounds inhibit NO production, although NS1 can also inhibit NOS-mediated ROS formation since NS1 blocks electron transfer through NOS by competitively inhibiting the binding of NADPH (or NT) [17,18]. Altogether, the protective effects of L-NAME/NS1 and the absence of NAC effect suggest that the photoinduced mechanism of cell death by NT_{2-4}/NT_{2-5} is actually eNOS-dependent and most likely due to a burst of NO. The absence of any NT fluorescence signal in HeLa cells, a cell line that does not express eNOS, as well as the absence of any photocytotoxic effect in NT-treated HeLa cells, regardless of the NT (Fig. S1), reinforces the relationship existing between the intracellular brightness of NTs and their ability to photoinduce a NOS-dependent cell death process.

3.3. eNOS-dependent and -independent photobleaching of NTs

Interestingly, during the time course of two-photon imaging experiments with HUVECs, we consistently observed a significant and continuous decrease of NT fluorescence emission, regardless of the compound. Reasoning that, at least a part of photobleaching could be related to the electron transfer process, we next monitored and quantitatively compared the photobleaching rates of NTs in HUVECs under continuous two-photon excitation, in the absence or presence of NS1/L-NAME.

As shown in Fig. 6A, all compounds were susceptible to photobleaching (confirming qualitative observations), however to different extents: NT_{2-5} > NT_{2-4}/NT_{2-7}/NT_{2-9} > NT_{2-3} > NT_{2-2}. Photobleaching experiments of the four most susceptible compounds (NT_{2-4}, NT_{2-5}, NT_{2-7} and NT_{2-9}) were repeated in the presence of NOS inhibitors in order to discriminate the part of photobleaching related to a "non-specific" process (*e.g.* photodegradation or NOS-independent photooxidation of

NTs) from the part related to a "specific" NOS-dependent photooxidation, as both processes can lead to a net loss of fluorescence emission intensity. HUVECs were then treated with NTs in the presence or absence of L-NAME or NS1, and further subjected to two-photon irradiation (Fig. 6B-E). L-NAME had no influence on photobleaching kinetics, regardless of the NT compound. However, a significant protective effect of NS1 was observed for NT_{2-4}/NT_{2-5} but not for NT_{2-7}/NT_{2-9} samples. Although L-NAME and NS1 are both eNOS inhibitors that efficiently inhibit the photocytotoxicity of NT_{2-4}/NT_{2-5}, their effect on photobleaching is clearly different. Only NS1 significantly influenced the photobleaching rate, according to its mechanism of action. Indeed, NS1, but not L-NAME, competes with NT_{2-4}/NT_{2-5} for binding to the NADPH-binding site in the NOS reductase domain and could then prevent any photoinduced electron transfer from the excited NT to the FAD group. By contrast, L-NAME that inhibits NO production by targeting the oxygenase domain, remains compatible with both (i) efficient binding of NT to the reductase domain and (ii) photoinduced oxidation of NT. These results show a strong correlation between the ability of NT_{2-4}/NT_{2-5} to trigger eNOS-dependent cell death (counteracted by L-NAME and NS1) and the eNOS-mediated photobleaching of NT_{2-4}/NT_{2-5}, originating from their photoinduced oxidation (= the part of photobleaching counteracted by NS1). By contrast, the observed photobleaching of NT_{2-7}/NT_{2-9} is fully explained by "non-specific" processes as shown by the absence of any protective effect of NS1. In conclusion, although all NTs were susceptible to general (non-specific) photobleaching effects, only NT_{2-4} and NT_{2-5} account for a specific NOS-dependent photooxidation.

3.4. Photoactivation of NT_{2-4}/NT_{2-5} triggers eNOS-dependent production of NO in HUVECs

To demonstrate that the photoinduced electron flow, specifically observed in the presence of NT_{2-4}/NT_{2-5}, actually leads to NO production, we used a fluorescent and selective NO probe composed of a NO-binding group (2-amino-3'-dimethylaminobiphenyl: AD) and a BODIPY dye [23]. The AD moiety also acts as a quencher of the BODIPY fluorescence in the absence of NO and its reaction with NO leads to fluorescence recovery. HUVECs were then simultaneously treated with NTs and the BODIPY-derived NO probe and subjected or not to light irradiation; NO production was finally evaluated in cell lysates by monitoring fluorescence emission (Fig. 7). Two different concentrations of the NO probe were used, leading to similar conclusions (compare panels A & B). No fluorescence enhancement was observed in the absence of photoactivation, regardless of the NT (compare with DMSO alone). By contrast, photoactivation of NT_{2-4} or NT_{2-5} (but not NT_{2-7} that is unable to induce cell death) led to significant fluorescence enhancement (≈1.31-1.36 for 5 μM NT). This enhancement factor was dependent on the initial concentration of NT as it was further increased using 10 μM NT (≈1.45). Moreover, treatments with L-NAME or NS1 totally abolished the fluorescence enhancement of the NO probe upon photoactivation of NT_{2-4}/NT_{2-5}, showing that these two NTs specifically trigger NO production in an eNOS-dependent manner. The concentration of produced NO was estimated based on fluorescence enhancement factors and calibration experiments using the DEA-NONOate as a NO donor (Fig. S4). NO concentrations of ≈2-2.4 μM and 6.5 μM were estimated, starting from initial NT concentrations of 5 and 10 μM, respectively, giving apparent NO production yields comprised between 40 and 65%, although the possibility of NT recycling after photooxidation in the cell context and the precise reaction stoichiometry remain to be determined.

The pro-apoptotic effect of NO in this concentration range is well established in HUVECs [43-45]. Unlike macrophages or other iNOS-expressing cells that produce large amounts of NO as a physiological response to pathogens or stresses, HUVECs do not have sufficient cytoprotective mechanisms (such as the Nrf2-dependent response) to escape from NO-induced apoptosis [46]. In HUVECs as well as in many other cell types, exposure to NO above ≈0.5 μM triggers a rapid activation of the p53 tumor suppressor and subsequent cell death by apoptosis [45,47]. The similar NO production upon NT_{2-4} and NT_{2-5} photoactivation parallels their similar photocytotoxicity properties as shown in microscopy and MTT experiments. This indicates that the different nature of the terminal electron donor group ($–NH_2$ or $–NHCH_3$) does not lead to a significant difference in terms of efficacy at the cellular level. The structural feature for efficacy that is common to NT_{2-4}/NT_{2-5} is the presence of a single carboxymethyl group, on the 3'-position of the ribose in the adenosine moiety. Taking into account that (i) all NTs (except NT_{2-9}) display similar affinities for the recombinant eNOS [22] and (ii)

only $NT_{2\text{-}4}$/$NT_{2\text{-}5}$ strongly colocalize with the Golgi apparatus, the specific influence of the 3'-carboxymethyl group in the cell context could be more related to intracellular routing properties, *i.e.* transport to the Golgi apparatus.

4. Conclusions

We found that the photoactivation of NTs having one carboxymethyl group on the 3'-position of the ribose, efficiently triggers electron flow and subsequent intracellular NO production at the eNOS level. Such a photoactivation is compatible with both one- (UV/visible light) and two-photon (NIR light) excitation processes and can lead to the formation of toxic micromolar concentrations of NO, underlying their potential use in generating apoptosis in tumor cells. However, further studies are needed to finely tune the NO production, typically below the toxic threshold (by decreasing NT concentration and/or light irradiation dose), to be able to modulate NO-dependent physiological processes occurring in the sub- to low-nanomolar concentration range such as eNOS-mediated functions in the cardiovascular system that are mainly dependent on the soluble guanylate cyclase activation by NO and the consecutive activation of cGMP-dependent effectors [48]. In this context, NTs could be potent modulators of NO-dependent functions such as regulation of vascular tone, angiogenesis or platelet thrombus formation.

Conflicts of interest

The authors have no conflicts of interest to declare.

Author contributions

N.H.N. and N.B. synthesized NT derivatives and the NO probe. J.-L.B. synthesized NS1. R.C., B.C. and P.T. performed two-photon microscopy experiments (cell death imaging, colocalization and photobleaching). R.C. and F.S. performed MTT tests. A.C. and F.S. performed measurements of NO production. A.S.-S., J.X. and E.D. designed the NT compounds and the experiments. E.D. and R.C. wrote the manuscript. All of the authors analysed data, discussed the experiments and commented on the manuscript.

Funding

This work was supported by the Agence Nationale de la Recherche [ANR-14-CE06-0031]; the Université Paris-Saclay (IRS BIOPROBE); and the government of Vietnam (to N.H.N.).

Appendix A. Supplementary data

Two-photon imaging of NT-treated HeLa cells; DIC transmission images corresponding to Fig. 2A; imaging of ROS production in NT-treated HUVECs; *in vitro* characterization of the fluorescence enhancement property of the BODIPY-derived NO probe.

References

[1] S. Moncada, Nitric oxide: discovery and impact on clinical medicine, J. R. Soc. Med. 92 (1999) 164-169.
[2] P. Pacher, J.S. Beckman, L. Liaudet, Nitric oxide and peroxynitrite in health and disease, Physiol. Rev. 87 (2007) 315-424.
[3] S. Godo, H. Shimokawa, Divergent roles of endothelial nitric oxide synthases system in maintaining cardiovascular homeostasis, Free Radic. Biol. Med. 109 (2017) 4-10.
[4] S. Kumar, R.K. Singh, T.R. Bhardwaj, Therapeutic role of nitric oxide as emerging molecule, Biomed. Pharmacother. 85 (2017) 182-201.

[5] H. Li, T.L. Poulos, Structure-function studies on nitric oxide synthases, J. Inorg. Biochem. 99 (2005) 293-305.
[6] M. Jáchymová, P. Martásek, S. Panda, L.J. Roman, M. Panda, T.M. Shea, Y. Ishimura, J.J. Kim, B.S. Masters, Recruitment of governing elements for electron transfer in the nitric oxide family, Proc. Natl. Acad. Sci. U. S. A. 102 (2005) 15833-15838.
[7] C. Feng, G. Tollin, M.A. Holliday, C. Thomas, J.C. Salerno, J.H. Enemark, D.K. Ghosh, Intraprotein electron transfer in a two-domain construct of neuronal nitric oxide synthase: the output state in nitric oxide formation, Biochemistry 45 (2006) 6354-6362.
[8] A.J. Dunford, S.E. Rigby, S. Hay, A.W. Munro, N.S. Scrutton, Conformational and thermodynamic control of electron transfer in neuronal nitric oxide synthase, Biochemistry 46 (2007) 5018-5029.
[9] R. Erkens, T. Suvorava, C.M. Kramer, L.D. Diederich, M. Kelm, M.M. Cortese-Krott, Modulation of Local and Systemic Heterocellular Communication by Mechanical Forces: A Role of Endothelial Nitric Oxide Synthase, Antioxid. Redox Signal. 26 (2017) 917-935.
[10] K.H. Lim, B.B. Ancrile, D.F. Kashatus, C.M. Counter, Tumour maintenance is mediated by eNOS, Nature 452 (2008) 646-649.
[11] J. Lahdenranta, J. Hagendoorn, T.P. Padera, T. Hoshida, G. Nelson, S. Kashiwagi, R.K. Jain, D. Fukumura, Endothelial nitric oxide synthase mediates lymphangiogenesis and lymphatic metastasis, Cancer Res. 69 (2009) 2801-2808.
[12] Z. Huang, J. Fu, Y. Zhang, Nitric oxide donor-based cancer therapy: advances and prospects, J. Med. Chem. 60 (2017) 7617−7635.
[13] S. Pfeiffer, E. Leopold, K. Schmidt, F. Brunner, B. Mayer, Inhibition of nitric oxide synthesis by NG-nitro-L-arginine methyl ester (L-NAME): requirement for bioactivation to the free acid, NG-nitro-L-arginine, Br. J. Pharmacol. 118 (1996) 1433-40.
[14] L. Rochette, J. Lorin, M. Zeller, J.-C. Guilland, L. Lorgis, Y. Cottin, C. Vergely, Nitric oxide synthase inhibition and oxidative stress in cardiovascular diseases: possible therapeutic targets? Pharmacol. Ther. 140 (2013) 239-257.
[15] O.E. Kıroğlu, Ö.Y. Özü, M. Emre, İ. Bayel, E.K. Kumcu, M.A. Seçilmiş, Residual NO modulates contractile responses and membrane potential in isolated rat mesenteric arteries, Nitric Oxide 71 (2017) 21-26.
[16] D.J. Stuehr, O.A. Fasehun, N.S. Kwon, S.S. Gross, J.A. Gonzalez, R. Levi, C.F. Nathan, Inhibition of macrophage and endothelial cell nitric oxide synthase by diphenyleneiodonium and its analogs, FASEB J. 5 (1991) 98-103.
[17] Y. Li, H. Wang, B. Tarus,, M. Romero-Perez, L. Morellato, E. Henry, V. Berka, A.L. Tsai, B. Ramassamy, H. Dhimane, C. Dessy, P. Tauc, J.-L. Boucher, E. Deprez, A. Slama-Schwok, Rational design of a fluorescent NADPH derivative imaging constitutive nitric-oxide synthases upon two-photon excitation, Proc. Natl. Acad. Sci. U. S. A. 109 (2012) 12526-12531.
[18] F. Rouaud, M. Romero-Perez, H. Wang, I. Lobysheva, B. Ramassamy, E. Henry, P. Tauc, D. Giacchero, J.-L. Boucher, E. Deprez, S. Rocchi, A. Slama-Schwok, Regulation of NADPH-dependent Nitric Oxide and reactive oxygen species signalling in endothelial and melanoma cells by a photoactive NADPH analogue, Oncotarget 5 (2014) 10650-10664.
[19] P.C. Ford, Photochemical delivery of nitric oxide, Nitric Oxide 34 (2013) 56-64.
[20] E. Beaumont, J.-C.,Lambry, C. Gautier, A. Robin, S. Gmouh, V. Berka, A.L. Tsai, M. Blanchard-Desce, A. Slama-Schwok, Synchronous photoinitiation of endothelial NO synthase activity by a nanotrigger targeted at its NADPH site, J. Am. Chem. Soc.129 (2007) 2178-2186.
[21] E. Beaumont, J.C. Lambry, M. Blanchard-Desce, P. Martasek, S.P. Panda, E.E. van Faassen, J.-C. Brochon, E. Deprez, A. Slama-Schwok, NO formation by neuronal NO-synthase can be controlled by ultrafast electron injection from a nanotrigger, Chembiochem. 10 (2009) 690-701.
[22] N.H. Nguyen, N. Bogliotti, R. Chennoufi, E. Henry, P. Tauc, E. Salas, L.J. Roman, A. Slama-Schwok, E. Deprez, J. Xie, Convergent synthesis and properties of novel photoactive NADPH mimics targeting nitric oxide synthases, Org. Biomol. Chem. 14 (2016) 9519-9532.
[23] X. Lv, Y. Wang, S. Zhang, Y. Liu, J. Zhang, W. Guo, A specific fluorescent probe for NO based on a new NO-binding group, Chem. Commun. 50 (2014) 7499-7502.

[24] P. Martinive, F. Defresne, E. Quaghebeur, G. Daneau, N. Crokart, V. Grégoire, B. Gallez, C. Dessy, O. Feron, Impact of cyclic hypoxia on HIF-1alpha regulation in endothelial cells--new insights for anti-tumor treatments, FEBS J. 276 (2009) 509-518.
[25] K.W. Dunn, M.M. Kamocka, J.H. McDonald, A practical guide to evaluating colocalization in biological microscopy, Am. J. Physiol. Cell Physiol. 300 (2011) 723–742.
[26] J. Schindelin, I. Arganda-Carreras, E. Frise, V. Kaynig, M. Longair, T. Pietzsch, S. Preibisch, C. Rueden, S. Saalfeld, B. Schmid, J.Y. Tinevez, D.J. White, V. Hartenstein, K. Eliceiri, P. Tomancak, A. Cardona, Fiji: an open-source platform for biological-image analysis, Nat. Methods 9 (2012) 676-682.
[27] R. Chennoufi, H. Bougherara, N. Gagey-Eilstein, B. Dumat, E. Henry, F. Subra, F. Mahuteau-Betzer, P. Tauc, M.-P. Teulade-Fichou, E. Deprez, Differential behaviour of cationic triphenylamine derivatives in fixed and living cells, Chem. Commun. 51 (2015) 14881-14884.
[28] R. Chennoufi, H. Bougherara, N. Gagey-Eilstein, B. Dumat, E. Henry, F. Subra, S. Bury-Moné, F. Mahuteau-Betzer, P. Tauc, M. P. Teulade-Fichou, E. Deprez, Mitochondria-targeted triphenylamine derivatives activatable by two-photon excitation for triggering and imaging cell apoptosis, Sci. Rep. (2016) 6:21458.
[29] A. Gautier, C. Gauron, M. Volovitch, D. Bensimon, L. Jullien, S. Vriz, How to control proteins with light in living systems, Nat. Chem. Biol. 10 (2014) 533-541.
[30] X. Wang, X. Chen, Y. Yang, Spatiotemporal control of gene expression by a light-switchable transgene system, Nat. Methods 9 (2012) 266-269.
[31] Y. Lyu, D. Cui, H. Sun, Y. Miao, H. Duan, K. Pu, Dendronized semiconducting polymer as photothermal nanocarrier for remote activation of gene expression, Angew. Chem. Int. Ed. 56 (2017) 9155-9159.
[32] Y. Lyu, J. Tian, J. Li, P. Chen, K. Pu, Semiconducting polymer nanobiocatalysts for photoactivation of intracellular redox reactions, Angew. Chem. Int. Ed. 57 (2018) 13484-13488.
[33] S.H. Lee, D.S. Choi, S.K. Kuk, C.B. Park, Photobiocatalysis: activating redox enzymes by direct or indirect transfer of photoinduced electrons, Angew. Chem. Int. Ed. 57 (2018) 7958-7985.
[34] D. Fulton, J. Fontana, G. Sowa, J.P. Gratton, M. Lin, K.X. Li, B. Michell, B.E. Kemp, D. Rodman, W.C. Sessa, Localization of endothelial nitric-oxide synthase phosphorylated on serine 1179 and nitric oxide in Golgi and plasma membrane defines the existence of two pools of active enzyme, J. Biol. Chem. 277 (2002) 4277-4284.
[35] F.A. Sanchez, R. Rana, D.D. Kim, T. Iwahashi, R. Zheng, B.K. Lal, D.M. Gordon, C.J. Meininger, W.N. Duran, Internalization of eNOS and NO delivery to subcellular targets determine agonist-induced hyperpermeability, Proc. Natl. Acad. Sci. U. S. A. 106 (2009) 6849-6853.
[36] J. Ousingsawat, P. Wanitchakool, A. Kmit, A.M. Romao, W. Jantarajit, R. Schreiber, K. Kunzelmann, Anoctamin 6 mediates effects essential for innate immunity downstream of P2X7 receptors in macrophages, Nat. Commun. (2015) 6:6245.
[37] G.R. Wickman, L. Julian, K. Mardilovich, S. Schumacher, J. Munro, J. Rath, S.A. Zander, A. Mleczak, D. Sumpton, N. Morrice, W.V. Bienvenut, M.F. Olson, Blebs produced by actin-myosin contraction during apoptosis release damage-associated molecular pattern proteins before secondary necrosis occurs, Cell Death Differ. 20 (2013) 1293-1305.
[38] Y. Xia, V.L. Dawson, T.M. Dawson, S.H. Snyder, J.L. Zweier, Nitric oxide synthase generates superoxide and nitric oxide in arginine-depleted cells leading to peroxynitrite-mediated cellular injury, Proc. Natl. Acad. Sci. U. S. A. 93 (1996) 6770-6774.
[39] M. Ott, V. Gogvadze, S. Orrenius, B. Zhivotovsky, Mitochondria, oxidative stress and cell death, Apoptosis 12 (2007) 913-922.
[40] A.A. Pieper, A. Verma, J. Zhang, S.H. Snyder, Poly (ADP-ribose) polymerase, nitric oxide and cell death, Trends Pharmacol. Sci. 20 (1999) 171-181.
[41] W. Li, W. Han, Y. Ma, L. Cui, Y. Tian, Z. Zhou, H. Wang, P53-dependent miRNAs mediate nitric oxide-induced apoptosis in colonic carcinogenesis, Free Radic. Biol. Med. 85 (2015) 105-113.
[42] E. Henry, N. Fung, J. Liu, G. Drakakaki, G. Coaker, Beyond glycolysis: GAPDHs are multi-functional enzymes involved in regulation of ROS, autophagy, and plant immune responses, PLoS Genet. 11 (2015) e1005199.

[43] Y.H. Shen, X.L. Wang, D.E. Wilcken, Nitric oxide induces and inhibits apoptosis through different pathways, FEBS Let. 433 (1998) 125-131.
[44] P. Pacher, J.S. Beckman, L. Liaudet, Nitric oxide and peroxynitrite in health and disease, Physiol. Rev. 87 (2007) 315-424.
[45] R.V. Mula, D. Machiah, L. Holland, X. Wang, H. Parihar, A.C. Sharma, P. Selvaraj, R. Shashidharamurthy, Immune Complex-Induced, Nitric Oxide-Mediated Vascular Endothelial Cell Death by Phagocytes Is Prevented with Decoy FcγReceptors, PloS One 11 (2016) e0153620.
[46] Z. Kovacevic, S. Sahni, H. Lok, M.J. Davies, D.A. Wink, D.R. Richardson, Regulation and control of nitric oxide (NO) in macrophages: Protecting the 'professional killer cell' from its own cytotoxic arsenal via MRP1 and GSTP1, Biochim. Biophys. Acta 1861 (2017) 995-999.
[47] D.D. Thomas, M.G. Espey, L.A. Ridnour, L.J. Hofseth, D. Mancardi, C.C. Harris, D.A. Wink, Hypoxic inducible factor 1alpha, extracellular signal-regulated kinase, and p53 are regulated by distinct threshold concentrations of nitric oxide, Proc. Natl. Acad. Sci. U. S. A. 101 (2004) 8894-8899.
[48] S.H. Francis, J.L. Busch, J.D. Corbin, D. Sibley, cGMP-dependent protein kinases and cGMP phosphodiesterases in nitric oxide and cGMP action, Pharmacol. Rev. 62 (2010) 525-563.

Figure legends.

Fig. 1. Chemical structures of NT_1 and second-generation compounds ($NT_{2\text{-}x}$). The 2-photon brightness values ($\sigma^2 x \Phi_F$) are indicated for each compound (from ref. [22]). σ^2 and Φ_F designate the 2-photon absorption cross-section and the fluorescence quantum yield, respectively. 1 GM = 10^{-50} $cm^4.s.photon^{-1}.molecule^{-1}$.

Fig. 2. Correlation between the two-photon brightness of NTs in living HUVECs and their colocalization with the Golgi apparatus. A) Two-photon fluorescence imaging of HUVECs pre-incubated with 5 μM NT for 2h at 37°C (λ_{ex}: 760 nm; emission slit: 450-550 nm); corresponding DIC transmission images are shown in Fig. S2. B) Quantitative analysis of intracellular NT fluorescence intensity. The bar graphs show mean ± SD values (30 cells analyzed per experiment). C) Colocalization of NTs with the Golgi apparatus in HUVECs. Top, imaging channel of NTs (λ_{ex}: 760 nm; emission slit: 450-550 nm). Middle, imaging channel of the BODIPY TR-ceramide Golgi tracker (λ_{ex}: 543 nm; emission slit: 570-720 nm). Bottom, corresponding merged images. Yellow-to-orange areas indicate NT/Golgi colocalization. To take into account the heterogeneous response between NTs in terms of fluorescence emission intensity, as shown in panels A-B, the PMT gains used for the NT channel in colocalization experiments were adjusted to obtain homogeneous emission intensities (see details in the Materials and Methods section). $NT_{2\text{-}6}$ was discarded from the study because of its relative chemical instability in culture medium [22]. D) Quantitative analysis of colocalization. tM1 and tM2 represent the Manders' Colocalization Coefficients (MCC) as explained in Materials and Methods.

Fig. 3. Differential effects of continuous two-photon irradiation of NTs on the appearance of membrane blebbing. Living HUVECs were pre-incubated without (no NT) or with 5 μM NT for 2h at 37°C and further subjected to continuous two-photon irradiation (760 nm; irradiance, 1.25 $W.cm^{-2}$) for 15 min (see Materials and Methods section for details). DIC transmission images are shown before (top) and after (bottom) the 15-min irradiation period. Among the different NTs, photoactivation of $NT_{2\text{-}4}$/$NT_{2\text{-}5}$ led to the appearance of plasma membrane blebs (indicated by blue arrows; yellow arrows point to examples of cell shrinkage). Enlarged fields of view are shown for these two compounds.

Fig. 4. Photocytotoxicity of NTs in HUVECs. Cell viability (in % of untreated cells) was determined by MTT assay for two different concentrations of NT (3 and 5 μM). HUVECs were treated with 1‰ DMSO (v/v) (= no NT) or NT ($NT_{2\text{-}4}$, $NT_{2\text{-}5}$ or $NT_{2\text{-}7}$) for 2h at 37°C and subjected (blue bars) or not (black bars) to light exposure (370±20 nm; irradiance, 6.6 $mW.cm^{-2}$) for 30 min (see Materials and Methods for details). For experiments in the presence of NOS inhibitors, HUVECs were pre-incubated

with 20 μM NS1 or 100 μM L-NAME for 30 min before addition of DMSO or NT. The bar graphs show mean ± SD values from three independent experiments (n=3) except for NT_{2-4} or NT_{2-5} (3 μM +/- light) (n=6), ***p<0.001, **p<0.01, NS: not significant.

Fig. 5. Effects of the antioxidant NAC and NOS inhibitors (L-NAME and NS1) on the NT-dependent appearance of membrane blebbing. Living HUVECs were treated as indicated in the Fig. 3 legend with 5 μM NT (NT_{2-4}, NT_{2-5} or NT_{2-7}), in the presence of NAC (A), L-NAME (B) or NS1 (C) (see Materials and Methods for details). HUVECs were then subjected to continuous two-photon irradiation (760 nm; irradiance, 1.25 $W.cm^{-2}$) for 15 min. DIC transmission images are shown before (top) and after (bottom) the 15-min irradiation period. DIC images of NT_{2-4}- or NT_{2-5}-treated cells obtained at t = 15 min show that both L-NAME and NS1, but not NAC, prevent both cell shrinkage and the appearance of plasma membrane blebs (blue and yellow arrows point to examples of membrane blebbing and cell shrinkage, respectively). NT_{2-7} which does not display any photocytotoxic effect was used here as a negative control.

Fig. 6. Intracellular photobleaching of NTs. Living HUVECs were pre-incubated with 5 μM NT for 2h at 37°C and further subjected to continuous 2-photon irradiation (760 nm; irradiance, 1.25 $W.cm^{-2}$) for 15 min (see Materials and Methods for details). A) Time course of NT fluorescence intensity in HUVECs. For each compound, fluorescence intensity values were normalized by the initial value (at time 0). B-E) Photobleaching experiments of NT_{2-4} (B), NT_{2-5} (C), NT_{2-7} (D) and NT_{2-9} (E) were repeated in the presence of L-NAME (100 μM) or NS1 (20 μM). The plots (representative data of three independent experiments for each NT) show that NS1 significantly reduces photobleaching of NT_{2-4}/NT_{2-5} only, whereas L-NAME has no effect on photobleaching, regardless of the NT.

Fig. 7. Measurement of NO production upon NT photoactivation in HUVECs. NO production was measured on cell extracts using 5 μM (A) or 0.5 μM (B) of the BODIPY-derived NO probe as explained in Materials and Methods. Top, total fluorescence intensity of the NO probe in the 500-530 nm range (λ_{ex}: 480 nm). Cells, treated with DMSO alone (1‰) or with NT_{2-4}, NT_{2-5} or NT_{2-7}, in the absence or presence of NOS inhibitors (L-NAME or NS1), were kept in the dark (black bars) or exposed to light (370±20 nm; irradiance, 1.6 $mW.cm^{-2}$) (white bars). The bar graphs show mean ± SD values from four independent experiments (n=4), except NS1 conditions (n=3); **p<0.01, *p<0.05, NS: not significant. Bottom, corresponding light/dark ratio (= fluorescence enhancement factor of the NO probe upon NT photoactivation). C) Representative emission spectra of the NO probe (5 μM) in different conditions (no light, light exposure +/- L-NAME or NS1). Unless specified, the NT concentration was 5 μM. L-NAME/NS1 concentrations, excitation/emission slits and PMT values are reported in Materials and Methods. In experiments with NS1, the emission spectrum of the NO probe was systematically corrected from the NS1 fluorescence contribution as explained in Materials and Methods.

NT_1

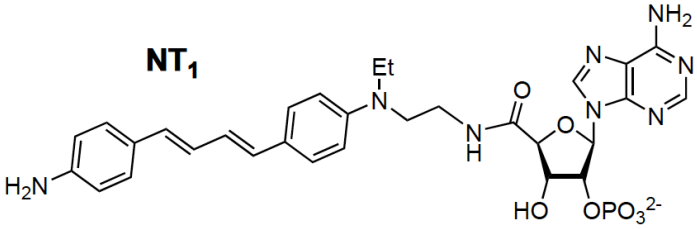

$NT_{2\text{-}x}$

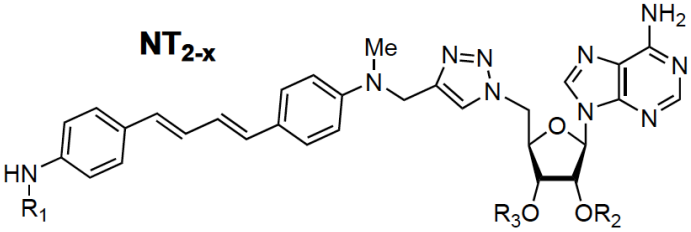

$NT_{2\text{-}x}$	R_1	R_2	R_3	$\sigma^2 \times \Phi_F$ (GM)
$NT_{2\text{-}2}$	CH_3	$-CH_2-CO_2H$	$-CH_2-CO_2H$	48
$NT_{2\text{-}3}$	H	$-CH_2-CO_2H$	$-CH_2-CO_2H$	54
$NT_{2\text{-}4}$	CH_3	-H	$-CH_2-CO_2H$	52
$NT_{2\text{-}5}$	H	-H	$-CH_2-CO_2H$	23
$NT_{2\text{-}6}$	CH_3	$-CH_2-CO_2H$	-H	43
$NT_{2\text{-}7}$	H	$-CH_2-CO_2H$	-H	28
$NT_{2\text{-}9}$	H	-H	-H	15

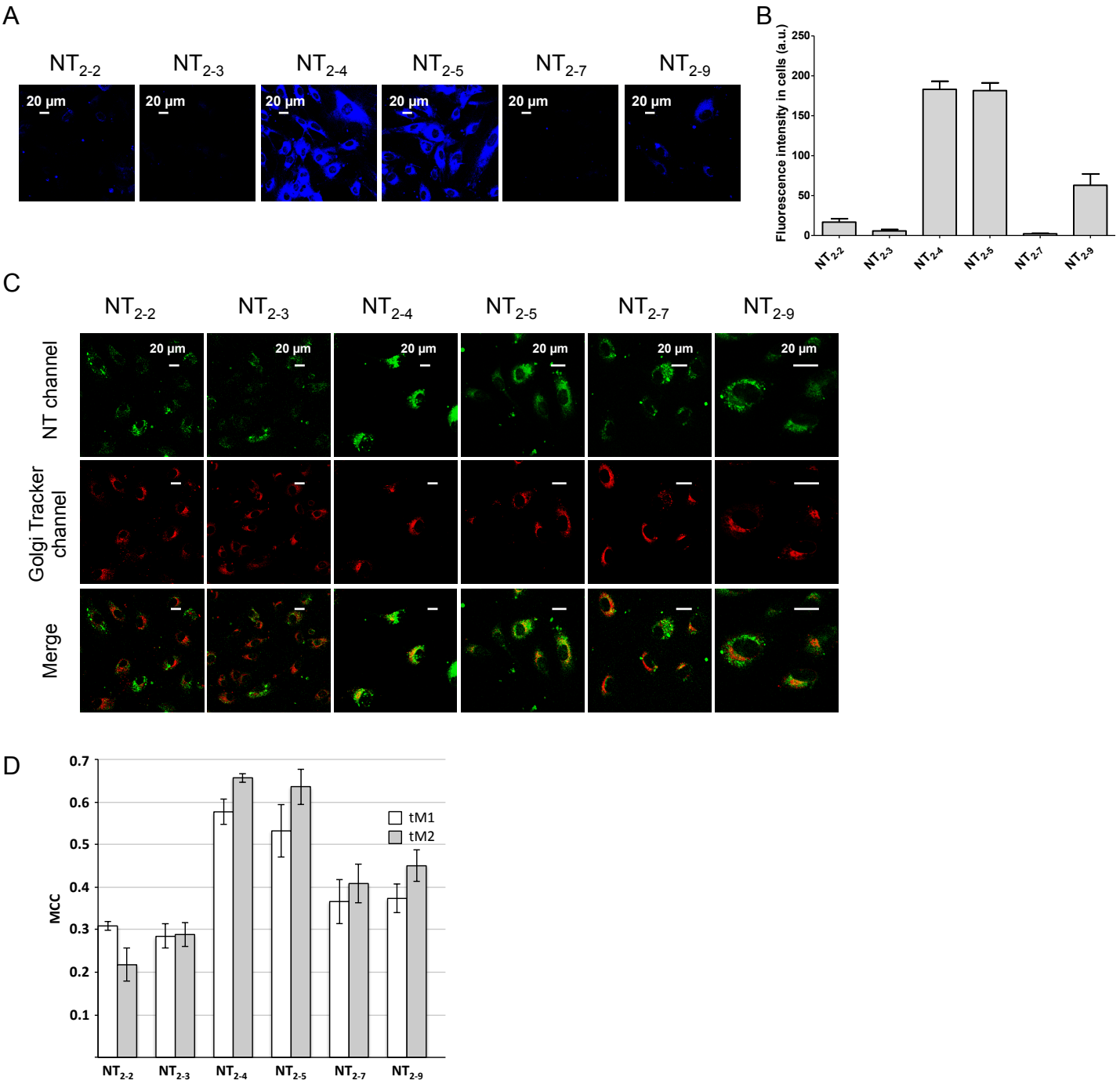
A
NT2-2
NT2-3
NT2-4
NT2-5
NT2-7
NT2-9
20 μm
B
Fluorescence intensity in cells (a.u.)
250
200
150
100
50
0
C
NT channel
Golgi Tracker channel
Merge
D
Mcc
0.7
0.6
0.5
0.4
0.3
0.2
0.1
tM1
tM2

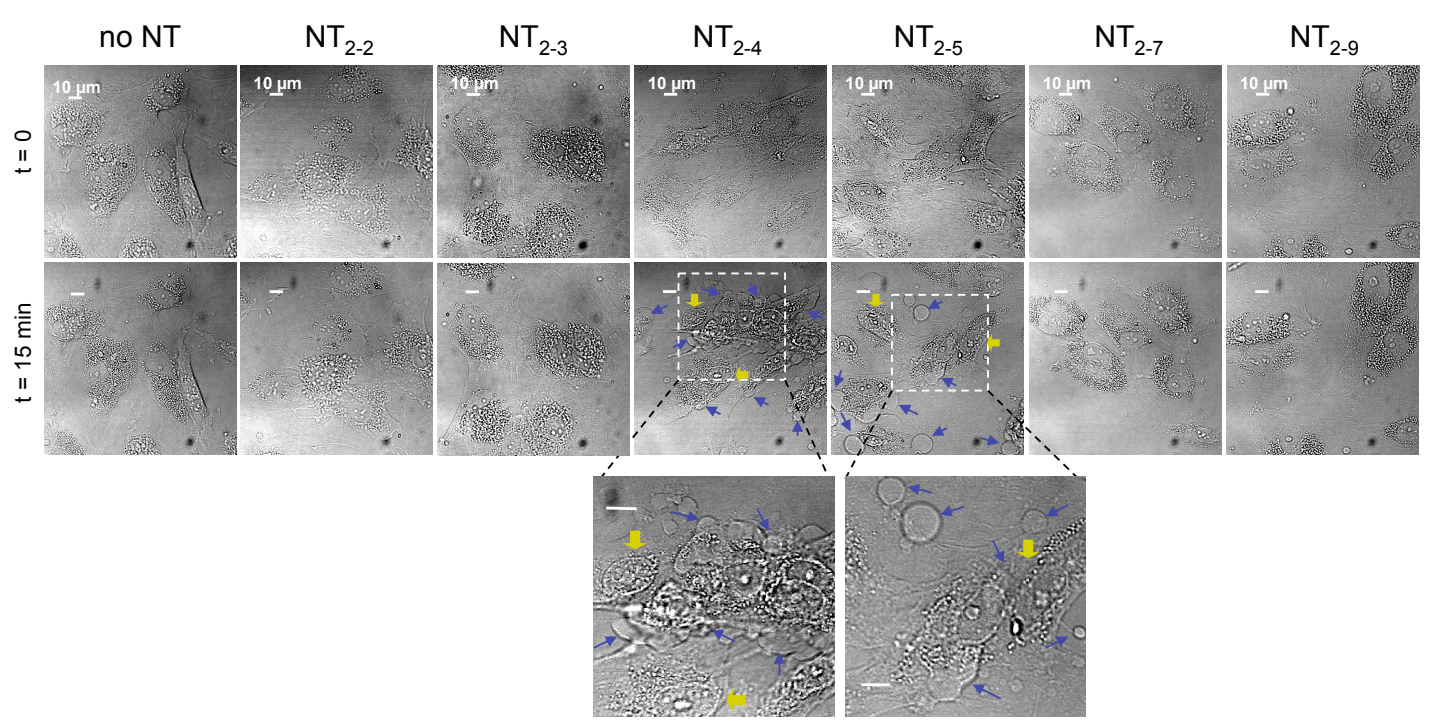
no NT
NT2-2
NT2-3
NT2-4
NT2-5
NT2-7
NT2-9
t = 0
t = 15 min
10 µm

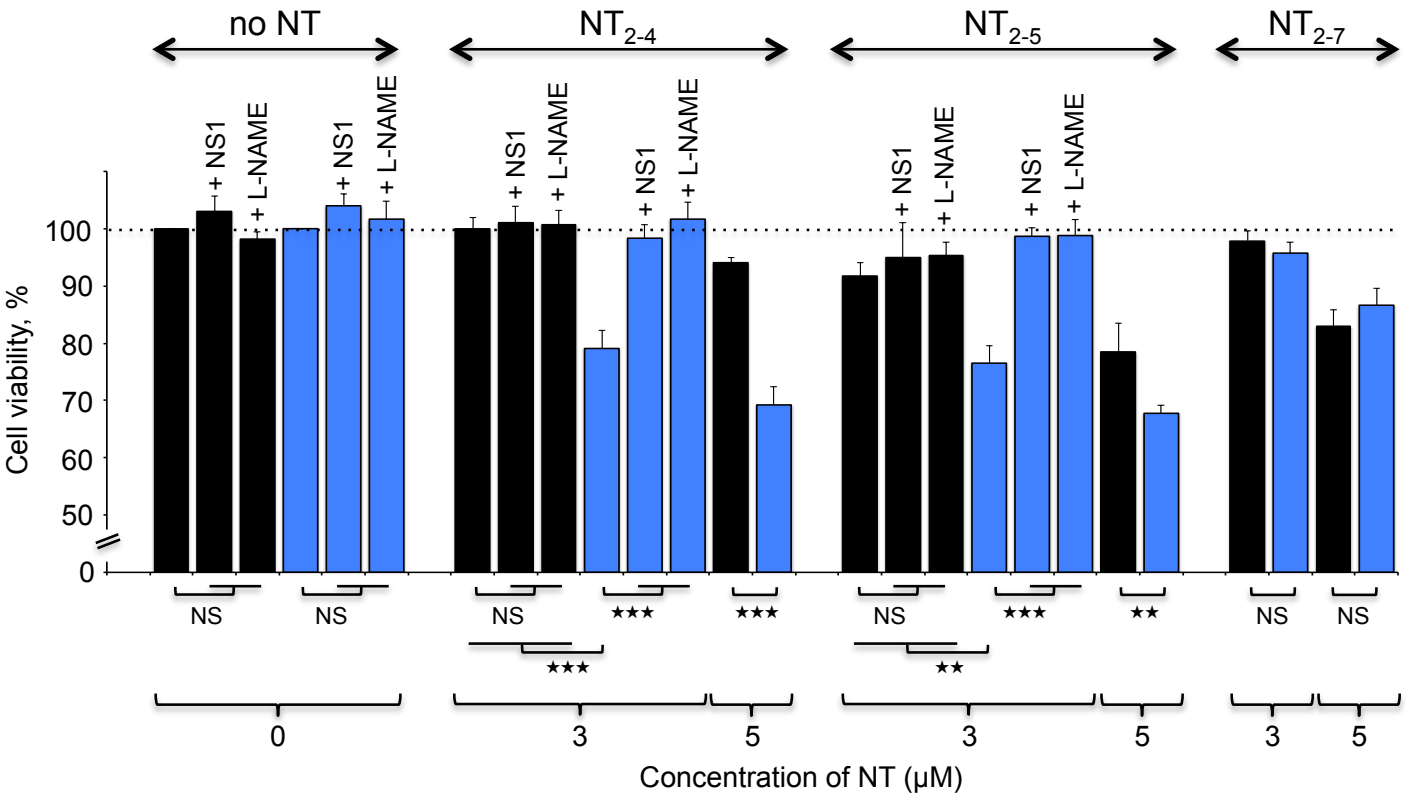
no NT
NT2-4
NT2-5
NT2-7
+ NS1
+ L-NAME
Cell viability, %
100
90
80
70
60
50
0
NS
★★★
★★
Concentration of NT (μM)

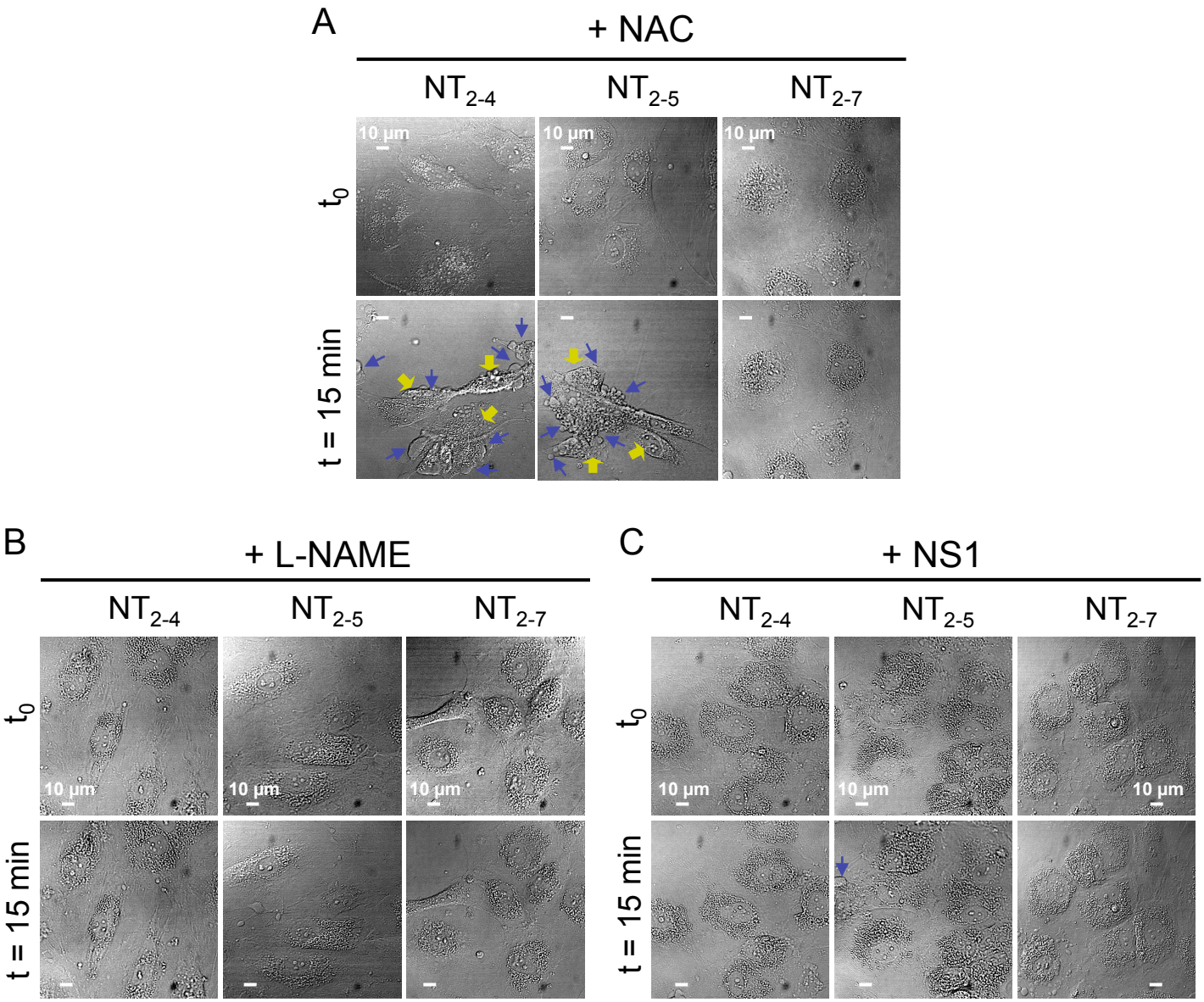
A
+ NAC
NT2-4
NT2-5
NT2-7
t0
t = 15 min
10 µm
B
+ L-NAME
NT2-4
NT2-5
NT2-7
t0
t = 15 min
10 µm
C
+ NS1
NT2-4
NT2-5
NT2-7
t0
t = 15 min
10 µm

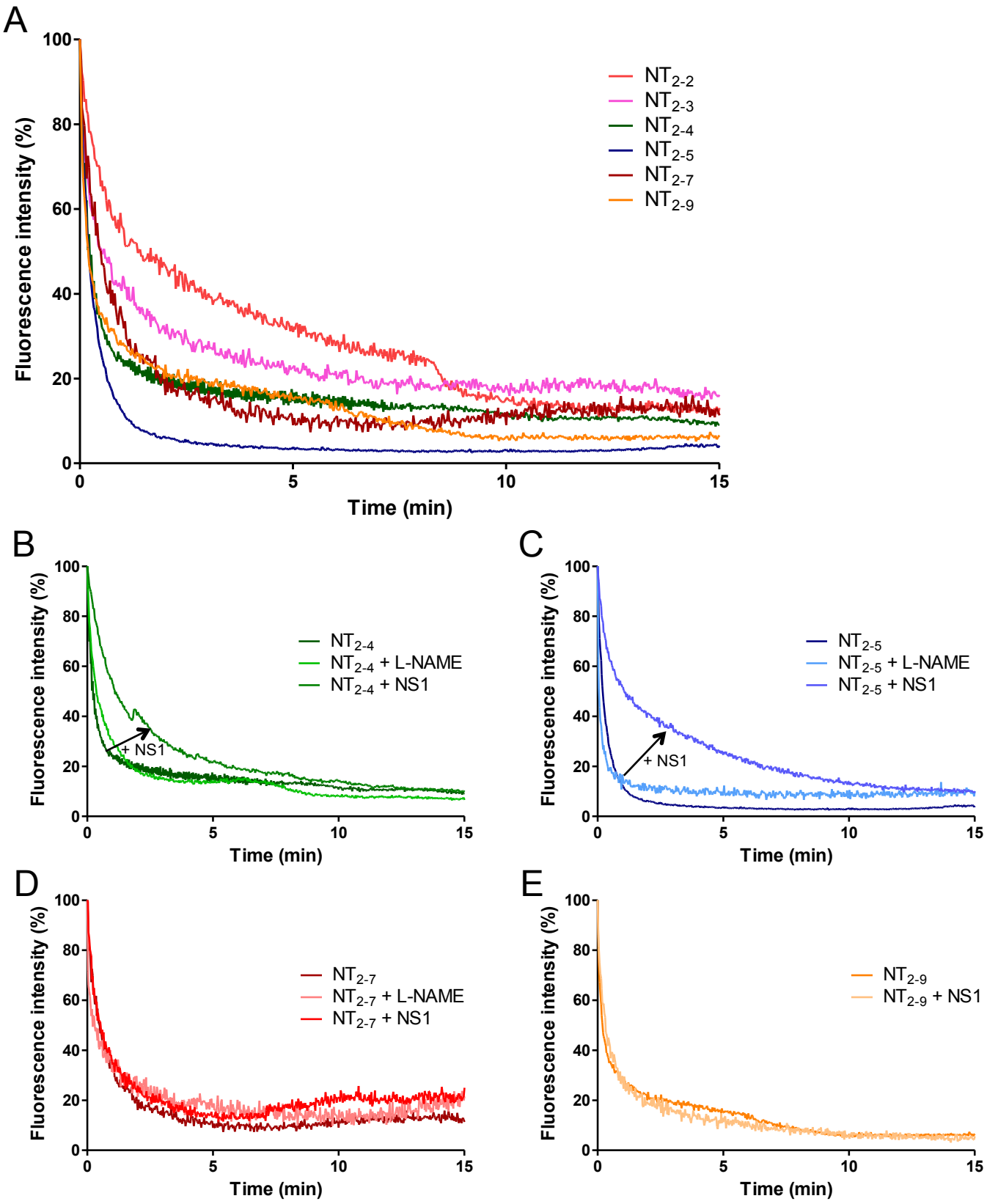
A
Fluorescence intensity (%)
Time (min)
NT2-2
NT2-3
NT2-4
NT2-5
NT2-7
NT2-9
B
NT2-4
NT2-4 + L-NAME
NT2-4 + NS1
+ NS1
C
NT2-5
NT2-5 + L-NAME
NT2-5 + NS1
+ NS1
D
NT2-7
NT2-7 + L-NAME
NT2-7 + NS1
E
NT2-9
NT2-9 + NS1

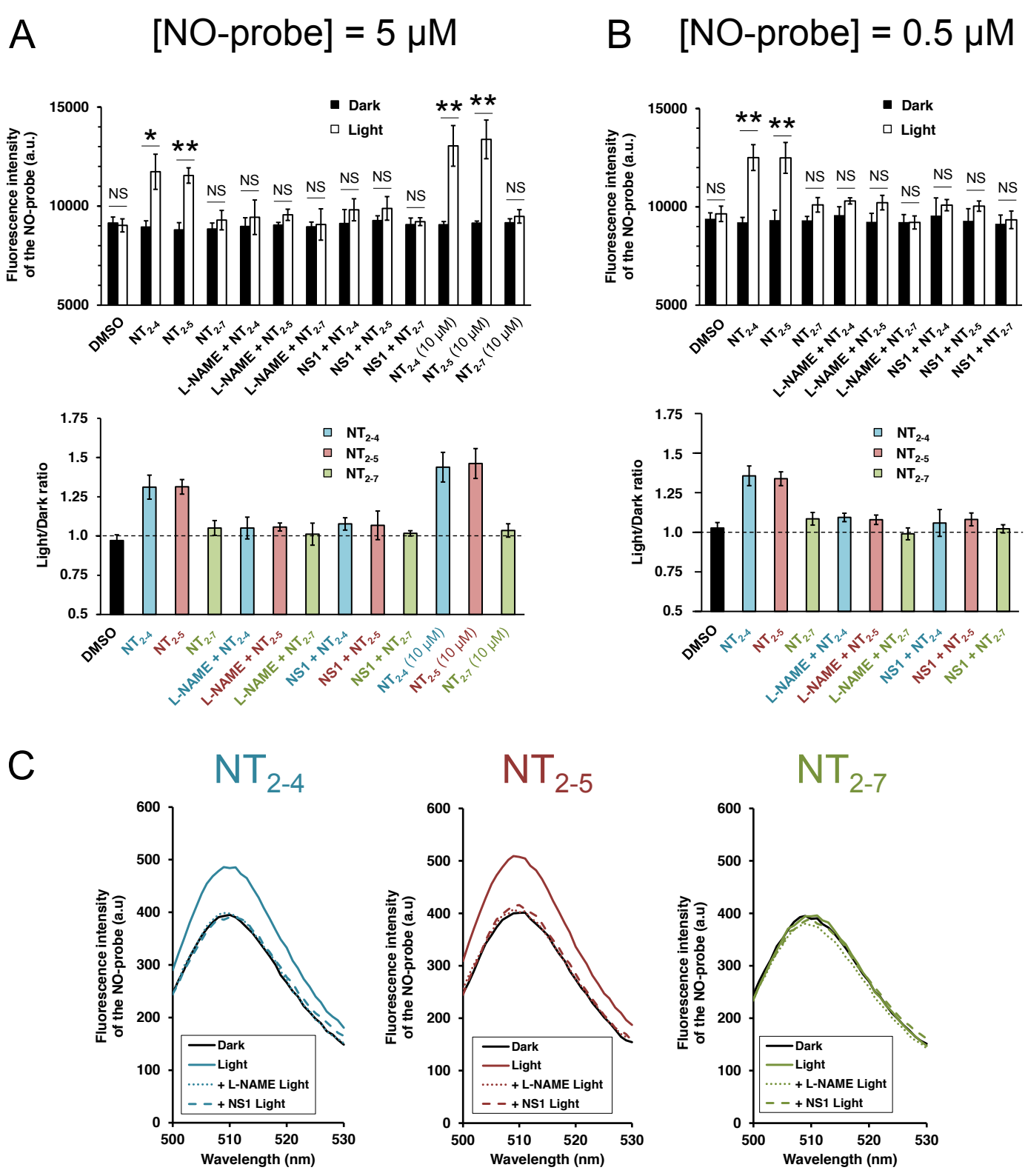
A
[NO-probe] = 5 μM
B
[NO-probe] = 0.5 μM
Fluorescence intensity of the NO-probe (a.u.)
Dark
Light
NS
*
**
DMSO
NT2-4
NT2-5
NT2-7
L-NAME + NT2-4
L-NAME + NT2-5
L-NAME + NT2-7
NS1 + NT2-4
NS1 + NT2-5
NS1 + NT2-7
NT2-4 (10 μM)
NT2-5 (10 μM)
NT2-7 (10 μM)
Light/Dark ratio
NT2-4
NT2-5
NT2-7
C
NT2-4
NT2-5
NT2-7
Fluorescence intensity of the NO-probe (a.u)
Dark
Light
+ L-NAME Light
+ NS1 Light
Wavelength (nm)

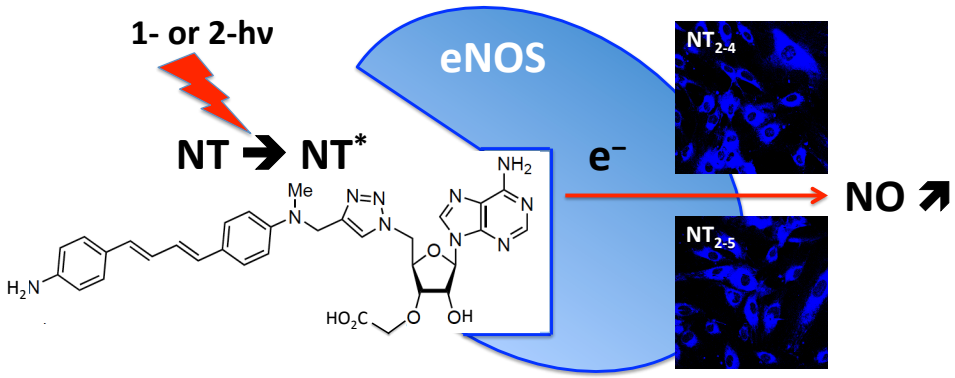
1- or 2-hv
NT → NT*
eNOS
e⁻
NO
NT2-4
NT2-5
NH2
Me
N=N
H2N
HO2C
O
OH